Electronic Supplementary Material (ESI) for Physical Chemistry Chemical Physics.

Supporting Information:

Inhibition Mechanism of SAHA in HDAC: A Revisit

Jingwei Zhou,[a] Ruibo Wu,*[a] and Hai-Bin Luo*[ab]

[a] School of Pharmaceutical Sciences, Sun Yat-sen University, Guangzhou 510006, P. R. China

[b] Collaborative Innovation Center of High Performance Computing, National University of Defense Technology, Changsha 410073, P. R. China

Main content	Corresponding Figure/Table		
	Text	SI	
Key Structural Basis	Figure 1	Figure S1	Table S1
Computational Methods	/	Figure S2	/
All Free Energy Profiles	Figure 2	Figure S3-S6	Table S2-S6
Metal-dependent Mechanism	Figure 3	Figure S7-S14	Table S7
The two water molecules (WAT1/2)	/	Figure S15-S18	Table S8-S10

Computational Methods

All computational models are shown in Table S2-S6. The HDAC2-SAHA (4LXZ),[1] HDAC8-SAHA (1T69)[2] and HDAC7-SAHA (3C0Z)[3] complex were used as the initial structures. The state-of-the-art Born-Oppenheimer *ab initio* quantum mechanics/molecular mechanics molecular dynamics (QM/MM MD)[4-10] method as well as combined with unbiased sampling and umbrella sampling[11, 12] technologies to capture all data presented in this work. The free energy profiles were mapped out by determining the probability distributions of the reaction coordinate and pieced together with WHAM[13, 14] program on the basis of the last 20 ps (25 ps for each window) QM/MM trajectories along the proton transfer reactions in all HDAC models.

Before the QM/MM simulations, the initial structures were first equilibrated for about 8 ns by employing AMBER 12.0 package[15]. And the detailed modeling protocol are similar to our previous work[10, 16-19]. During the QM/MM MD simulations, the different QM partition schemes were considered as shown in Table 2-6 and Figure S2. All the QM subsystems were treated by the B3LYP functional with the Stuttgart ECP/basis set (SDD)[20] for the zinc atom and the 6-31G* basis set for all other atoms. This level of QM treatment[5, 10, 16-19, 21-24] had been extensively tested and successfully employed to describe the zinc coordination shell, as well as had been employed in our previous and *Wiest*'s calculations for HDAC8[17, 25]. The MM subsystems were described by the Amber99SB[26-28] force field and the QM/MM boundaries were described by the pseudobond approach with the improved pseudobond parameters.[29-32] Other computational details are very similar to the previous QM/MM QM protocol[10, 18, 19]. All computations were performed in the modified Q-Chem[33] and Tinker[34] programs.

References

1. B. E. Lauffer, R. Mintzer, R. Fong, S. Mukund, C. Tam, I. Zilberleyb, B. Flicke, A. Ritscher, G. Fedorowicz, R. Vallero, D. F. Ortwine, J. Gunzner, Z. Modrusan, L. Neumann, C. Koth, P. J. Lupardus, J. S. Kaminker, C. E. Heise and P. Steiner, *J. Biol. Chem.*, 2013, **288**, 26926-26943.
2. J. R. Somoza, R. J. Skene, B. A. Katz, C. Mol, J. D. Ho, A. J. Jennings, C. Luong, A. Arvai, J. J. Buggy, E. Chi, J. Tang, B. C. Sang, E. Verner, R. Wynands, E. M. Leahy, D. R. Dougan, G. Snell, M. Navre, M. W. Knuth, R. V. Swanson, D. E. McRee and L. W. Tari, *Structure*, 2004, **12**, 1325-1334.
3. A. Schuetz, J. Min, A. Allali-Hassani, M. Schapira, M. Shuen, P. Loppnau, R. Mazitschek, N. P. Kwiatkowski, T. A. Lewis, R. L. Maglathin, T. H. McLean, A. Bochkarev, A. N. Plotnikov, M. Vedadi and C. H. Arrowsmith, *J. Biol. Chem.*, 2008, **283**, 11355–11363.
4. Y. Z. Zhou, S. L. Wang and Y. K. Zhang, *J. Phys. Chem. B*, 2010, **114**, 8817-8825.
5. R. Wu, P. Hu, S. Wang, Z. Cao and Y. Zhang, *J. Chem. Theory Comput.*, 2010, **6**, 337-343.
6. P. Hu, S. Wang and Y. Zhang, *J. Am. Chem. Soc.*, 2008, **130**, 3806–3813.
7. P. Hu, S. L. Wang and Y. K. Zhang, *J. Am. Chem. Soc.* , 2008, **130**, 16721–16728.
8. Z. H. Ke, Y. Z. Zhou, P. Hu, S. L. Wang, D. Q. Xie and Y. K. Zhang, *J. Phys. Chem. B*, 2009, **113**, 12750-12758.
9. S. L. Wang, P. Hu and Y. K. Zhang, *J. Phys. Chem. B*, 2007, **111**, 3758-3764.
10. R. Wu, S. Wang, N. Zhou, Z. Cao and Y. Zhang, *J. Am. Chem. Soc.*, 2010, **132**, 9471–9479.
11. G. M. Torrie and J. P. Valleau, *J. Comput. Phys.*, 1977, **23**, 187-199.
12. R. Vijayaraj, S. Van Damme, P. Bultinck and V. Subramanian, *J. Phys. Chem. B*, 2012, **116**, 9922-9933.
13. S. Kumar, D. Bouzida, R. H. Swendsen, P. A. Kollman and J. M. Rosenberg, *J. Comput. Chem.*, 1992, **13**, 1011-1021.
14. M. Souaille and B. Roux, *Comput. Phys. Commun.*, 2001, **135**, 40-57.
15. D. A. Case, T. A. Darden, I. Cheatham, T.E., C. L. Simmerling, J. Wang, R. E. Duke, R. Luo, R. C. Walker, W. Zhang, K. M. Merz, B. Roberts, S. Hayik, A. Roitberg, G. Seabra, J. Swails, A. W. Götz, I. Kolossváry, K. F. Wong, F. Paesani, J. Vanicek, R. M. Wolf, J. Liu, X. Wu, S. R. Brozell, T. Steinbrecher, H. Gohlke, Q. Cai, X. Ye, J. Wang, M.-J. Hsieh, G. Cui, D. R. Roe, D. H. Mathews, M. G. Seetin, R. Salomon-Ferrer, C. Sagui, V. Babin, T. Luchko, S. Gusarov, A. Kovalenko and P. A. Kollman, *AMBER 12, University of California, San Francisco.*, 2012.
16. N. H. Chen, J. W. Zhou, J. B. Li, J. Xu and R. B. Wu, *J. Chem. Theory Comput.*, 2014, **10**, 1109-1120.
17. R. Wu, Z. Lu, Z. Cao and Y. Zhang, *J. Am. Chem. Soc.*, 2011, **133**, 6110-6113.
18. J. W. Zhou, M. Li, N. H. Chen, S. L. Wang, H. B. Luo, Y. K. Zhang and R. B. Wu, *ACS Chem. Biol.*, 2015, **10**, 687-692.
19. J. W. Zhou, H. J. Xie, Z. H. Liu, H. B. Luo and R. B. Wu, *J. Chem. Inf. Model.*, 2014, **54**, 3162-3171.
20. M. Dolg, U. Wedig, U. Stoll and H. Preuss, *J. Chem. Phys.* , 1987, **86**, 866-872
21. S. F. Sousa, P. A. Fernandes and M. J. Ramos, *Biophys. J.*, 2005, **88**, 483-494.
22. S. F. Sousa, P. A. Fernandes and M. J. Ramos, *J. Am. Chem. Soc.*, 2007, **129**, 1378-1385.
23. C. Corminboeuf, P. Hu, M. E. Tuckerman and Y. K. Zhang, *J. Am. Chem. Soc.*, 2006, **128**, 4530-4531.
24. C. Y. Xiao and Y. K. Zhang, *J. Phys. Chem. B*, 2007, **111**, 6229-6235.

25. K. Chen, X. Zhang, Y. D. Wu and O. Wiest, *J. Am. Chem. Soc.*, 2014, **136**, 11636-11643.
26. W. D. Cornell, P. Cieplak, C. I. Bayly, I. R. Gould, K. M. Merz, D. M. Ferguson, D. C. Spellmeyer,T. Fox, J. W. Caldwell and P. A. Kollman, *J. Am. Chem. Soc.*, 1995, **117**, 5179-5197.
27. V. Hornak, R. Abel, A. Okur, B. Strockbine, A. Roitberg and C. Simmerling, *Proteins: Struct.,Funct., Bioinf.*, 2006, **65**, 712-725.
28. J. M. Wang, P. Cieplak and P. A. Kollman, *J. Comput. Chem.*, 2000, **21**, 1049-1074.
29. Y. K. Zhang, *J. Chem. Phys.*, 2005, **122**, 024114.
30. Y. K. Zhang, *Theor. Chem. Acc.*, 2006, **116**, 43-50.
31. Y. K. Zhang, T. S. Lee and W. T. Yang, *J. Chem. Phys.*, 1999, **110**, 46-54.
32. Y. K. Zhang, H. Y. Liu and W. T. Yang, *J. Chem. Phys.*, 2000, **112**, 3483-3492.
33. Y. Shao, L. F. Molnar, Y. Jung, J. O. C. Kussmann, S. T. Brown, A. T. Gilbert, L. V. Slipchenko, S. V. Levchenko, D. P. O'Neill, R. A. DiStasio, R. C. Lochan, T. Wang, G. J. Beran, N. A. Besley, J. M. Herbert, C. Y. Lin, T. Van Voorhis, S. H. Chien, A. Sodt, R. P. Steele, V. A. Rassolov, P. E. Maslen, P. P. Korambath, R. D. Adamson, B. Austin, J. Baker, E. F. Byrd, H. Dachsel, R. J. Doerksen, A. Dreuw, B. D. Dunietz, A. D. Dutoi, T. R. Furlani, S. R. Gwaltney, A. Heyden, S. Hirata, C. P. Hsu, G. Kedziora, R. Z. Khalliulin, P. Klunzinger, A. M. Lee, M. S. Lee, W. Liang, I. Lotan, N. Nair, B. Peters, E. I. Proynov, P. A. Pieniazek, Y. M. Rhee, J. Ritchie, E. Rosta, C. D. Sherrill, A. C. Simmonett, J. E. Subotnik, H. L. Woodcock, W. Zhang, A. T. Bell, A. K. Chakraborty, D. M. Chipman, F. J. Keil, A. Warshel, W. J. Hehre, H. F. Schaefer, J. Kong, A. I. Krylov, P. M. Gill and M. Head-Gordon, *Q-Chem,version 3.0,Q-chem,Inc.: Pittsburgh, PA.*, 2006.
34. J. W. Ponder, *TINKER, Software Tools for Molecular Design,Version 4.2.*, 2004.

More discussions on the two water molecules (WAT1/2)

Based on our simulations, it was found that the WAT2 would form hydrogen bond with the SAHA: O2 when the second metal ion was mutated to K^+ or removed in the HDAC2 as shown in Figure S15 and Table S8. While for the wild type HDAC2, the strong hydrogen bond between WAT2: H1 and Y308: OH would maintain at about 2.06 during the 20 ps QM/MM MD simulation. The coordination distance of Zn-SAHA: O2 kept at about 2.16 and WAT2: H1 was far away from the SAHA: O2 (3.16). However, when the Ca^{2+} ion was mutated to K^+, the hydrogen bond of WAT2: H1-Y308: OH become weaker (2.49) while the distance of Zn-SAHA: O2 (2.68) and WAT2: H1-SAHA: O2 (2.95) get longer and shorter, respectively. This local binding modes transition would become more obvious when the second metal ion was deleted as shown in Figure S15. When the Y308 residue was further mutated to His based on the $Ca^{2+}\rightarrow K^+$ mutant model, the WAT2: H1-Y308: OH hydrogen bond was totally broken, the Zn-SAHA: O2 (3.47) would become longer and the WAT2: H1 would form very strong hydrogen bond with SAHA: O2 (2.06). However, the hydrogen bond between WAT2: H1 and SAHA: O2 would not be formed if there was only Y308H mutant for HDAC2. It means that the second metal ion determines the functional role of the WAT2 on the deprotonation of SAHA. The similar results were also found in the HDAC8 wild type and mutant models (see Figure S16 and Table S8). In sum, the presence or absence of the hydrogen bond between Zn-SAHA: O2 and WAT2, which is relative to the proton transfer reaction of SAHA, is controlled by the "second metal site" in HDAC.

Due to the K^+ ion in the second metal site of HDAC8, the WAT2 could not only form hydrogen bond with the Y308, but also with SAHA: O2 as shown in Figure S16. Therefore there maybe exist two states for the HDAC8 (see Figure S17). The state A: WAT2: H1-Y306: OH hydrogen bond was formed; The state B: WAT2: H1-SAHA: O2 hydrogen bond was formed. Interestingly, the two states were indeed observed in crystals (state A: 4BZ6 and 4BZ7; state B: 4BZ9) and also reproduced in our simulations. Meanwhile, due to the existence of the Ca^{2+} ion in HDAC2 and K^+/H843

in HDAC7, only state A for HDAC2 (state A: 4LXZ) and only state B for HDAC7 (state B: 3COZ and 3C10) were found theoretically and experimentally. These highly unified results between computation and experiments further indicated that our proposed protonation mechanism is reliable. To further identify our proposed protonation state of SAHA in HDAC8/7/2, the coordination distance of Zn-SAHA: O1 and Zn-SAHA: O2 were compared between our computational results and crystal structures. As shown in Table S1 and S9, based on all the HDAC8-hydroxamate (SAHA belongs to hydroxamate) crystal structures, we can see the Zn-SAHA: O1 distance fluctuates among 1.90~2.50 while 1.90~3.00 for Zn-SAHA: O2. These statistical results were very close to the computational coordination distances of negative SAHA (2.18 and 2.70) in HDAC8. The similar consistency were also found in HDAC2 and HDAC7. Thus based on these simulations, deprotonation state of SAHA is favorable in the HDAC7 and HDAC8, while neutral or negative SAHA is not biased and undistinguished in HDAC2

Above proposed possible protonation state was based on the situation of the existence of the two crystal water (WAT1/2) or the solvent water enter into this water binding site in current modeling. However, except for HDAC2 in which the two crystal water (WAT1/2) were completely crystallized, the existence of the two crystal water was not guaranteed based on all available human-HDAC8 and HDAC7 crystals (only WAT1 or WAT2 were found in HDAC8 or HDAC7, respectively, as shown in Table S1). Thus it is necessary to identify the protonation mechanism if only one water in the "water binding site". For HDAC7, the case that only containing WAT2 (model 7-1) have been further considered carefully, in comparison with the model (model 7-2) in which both WAT1 and WAT2 existed, the stability difference between the neutral state and negative state was smaller (-3.1 vs -4.4 kcal/mol), but the proton transfer reaction was also facile (0.7 kcal/mol vs 0.3 kal/mol, see Table S6). Meanwhile, the 20 ps unrestricted QM/MM MD simulation indicated that the neutral state would only survive for 0.47 ps for HDAC7 (see Table S10). For the model of HDAC8-1T69, in which only WAT1 existed, the neutral SAHA was also unstable and could only survive for 2.12 ps and then transfer to be negative SAHA. Considering the "2V5X" structure

had a higher resolution than 1T69 (1T69 was 2.91 while 2V5X was 2.25Å), and the WAT1 was crystallized, we also performed similar QM/MM MD simulation on "2V5X" via modifying the ligand to be SAHA which was a SAHA-like inhibitor in the original crystal. As shown in Table S10, for HDAC8-2V5X model (only WAT1), the negative SAHA was also more stable than neutral one.

In sum, whatever both WAT1/2 are existed or only one (WAT1 or WAT2) existed in HDAC8/7, the negative SAHA is more stable and prevalent. Moreover, as we discussed in text, functional roles of Y306 in proton transfer reaction is relative to the "second metal site", the regulatory effect of "water binding site" on protonation of SAHA is also dependent on the "second metal site", thus further proved the fidelity of our proposed "Metal-dependent" mechanism. Furthermore, in the HDAC2-LLX and HDAC8-substrate crystals, the LLX (a selective Benzamide HDAC inhibitor) and substrate (Acetyl-Lysine) form a strong hydrogen bond with the conserved G154/151 via an acyl amino by precisely utilizing the WAT2 site (see Figure S1). It indicates that the WAT1/2 binding site could be applied to inhibitor design.

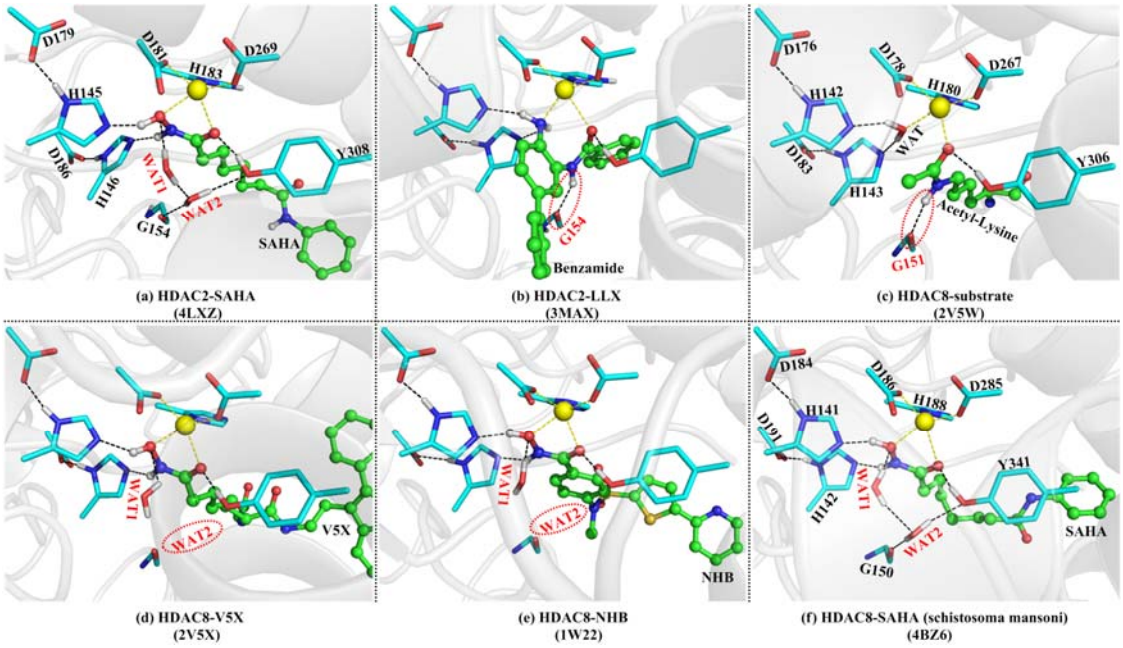

Figure S1. Illustration of the active site structure of the enzyme-inhibitor complex in HDAC2 (a & b) and HDAC8 (c, d, e and f). There is a distinct hydrogen bond network among zinc binding group, Y308, G154 and two water molecules (WAT1 and WAT2). In the HDAC2-LLX and HDAC8-substrate crystals, the LLX (a benzamide-like HDAC inhibitor) and substrate (Acetyl-Lysine) just precisely utilize the WAT2 site to form a strong hydrogen bond with the conserved G154/151 via an acyl amino. It indicated that the WAT1/2 could be applied to inhibitor design. In the HDAC8-substrate crystal the Y306F mutation is manually recovered. The non-human 4BZ6 crystal is a *schistosoma mansoni* HDAC8 (also for 4BZ7 and 4BZ9), whose active site is identical with human and have two waters in the second zinc coordination shell. Another two human HDAC8 crystals (1VKG and 3RQD) have one water (WAT1). The more details about WAT1/2 were shown in Table S1.

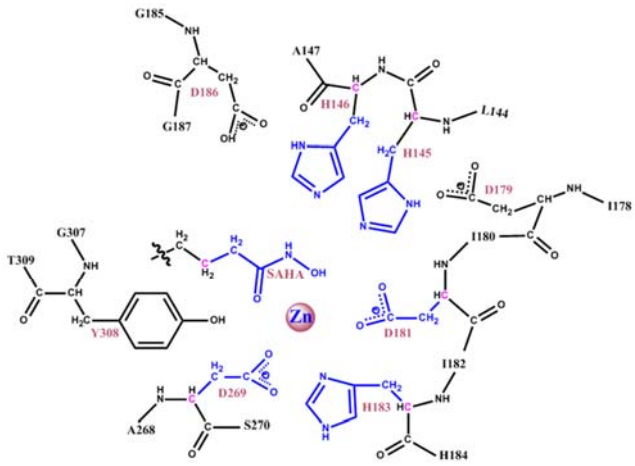

(a) Cs-QMS

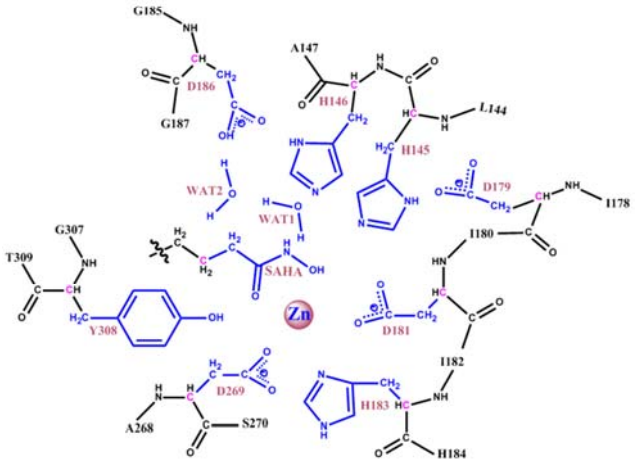

(b) BQMS
(BQMS= Cs-QMS+D-H Dyads+WAT1/2+Y308)

Figure S2. The detailed QM/MM partition schemes for *ab initio* QM/MM MD simulations in HDAC2-SAHA models (refer to Table S2 and S3). Black, MM subsystem; Pink, boundary carbon atoms which treated at QM level; Blue, the other atoms in QM subsystems. (a) represents the classical smallest QM subsystem (Cs-QMS); (b) represents the biggest QM subsystem (BQMS=Cs-QMS+D-H Dyads+WAT1/2 +Y308). The QM/MM partition schemes of HDAC8/7-SAHA models were similar to that of HDAC2-SAHA models and see details in Table S4-S6.

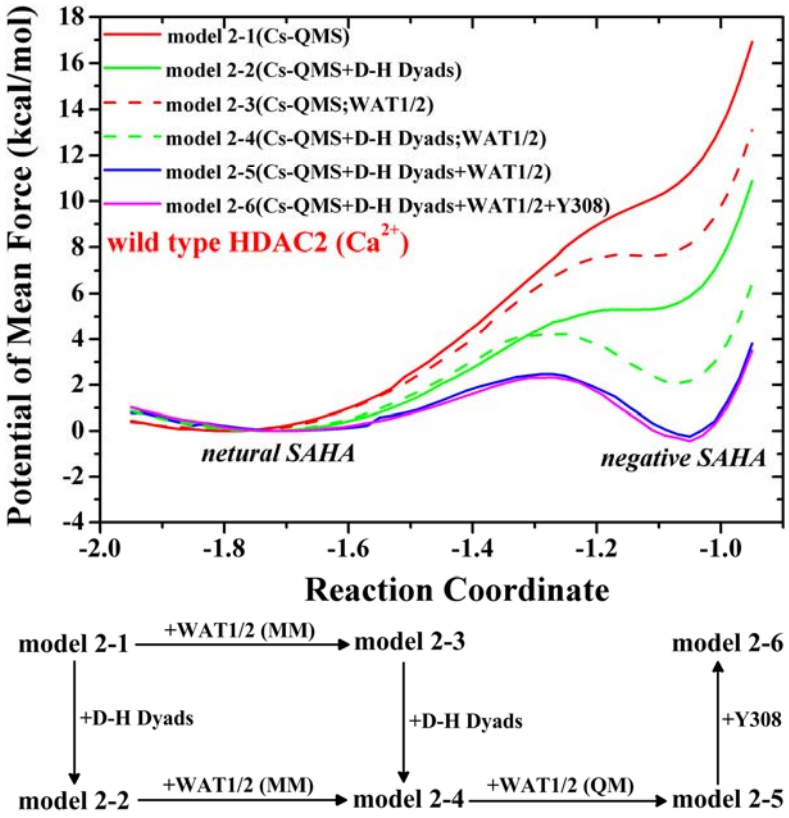

Figure S3. Benchmark test on free energy profiles of the proton transfer from SAHA to H145 in the wild types HDAC2 which refer to Table S2. The distance between the hydroxyl hydrogen of SAHA and the N^{ε} atom of H145 is chosen as the reaction coordinate. The QM subsystem of model 2-6 (colored by pink) represents the Biggest QM Subsystems (BQMS) which refer to Figure 2 (a) and Figure S2. The two conserved water molecules (WAT1/2, see Figure 1 and S1) were added into the MM subsystem based on the Cs-QMS (see Figure S2, model 2-1) and Cb-QMS (see Figure S2, model 2-2) to build the model 2-3 and model 2-4, respectively, while in the model 2-5 the WAT1/2 was partitioned into the QM subsystem based on the Cb-QMS model.

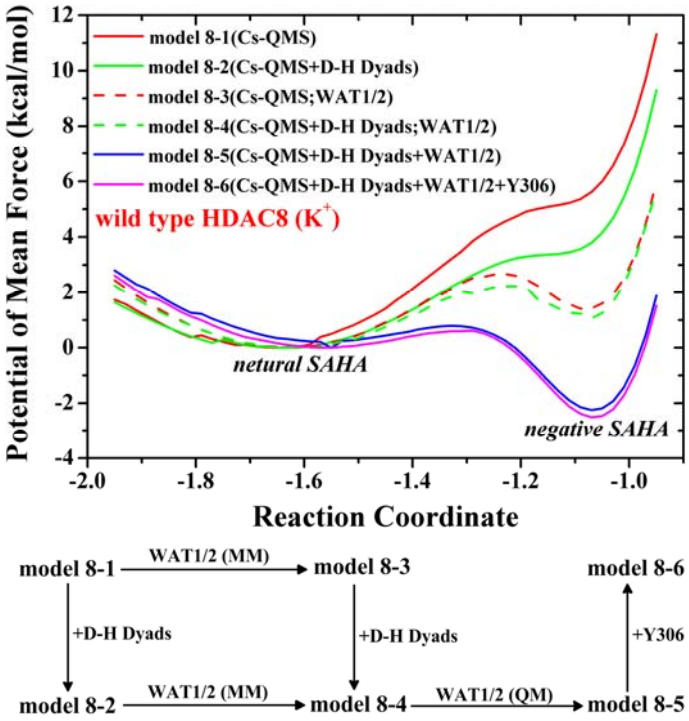

Figure S4. Benchmark test on free energy profiles of the proton transfer from SAHA to H142 in the wild types HDAC8 which refer to Table S4. The distance between the hydroxyl hydrogen of SAHA and the N^{ε} atom of H142 is chosen as the reaction coordinate. For model using the Classical smallest QM Subsystem (Cs-QMS, model 8-1, defined in our previous work for HDAC8), SAHA prefers to be neutral which is consistent with our previous conclusion. For model using Classical bigger QM Subsystem (Cs-QMS+D-H Dyads, model 8-2, defined as *Wiest's* work for HDAC8). Based on these PMF profiles, we strongly realized that characterize the reaction features based on free energy calculation is critical especially for proton transfer reaction with low barrier. Take model 8-2 as example, it is forbidden in view of current QM/MM free energy simulations (also for model 8-1 as what we used before), whereas it is spontaneous based on static QM/MM optimization as *Wiest* done (Ref. 9 in text). Therefore, we proposed that the prevalence of negative SAHA in HDAC8 in *Wiest*'s modeling (Ref. 18 in text) mostly due to the lack of K^+ (see model 8-10 in Figure S6) but not due to the bigger QM size used in comparison with our previous modeling (Ref. 4d in text).

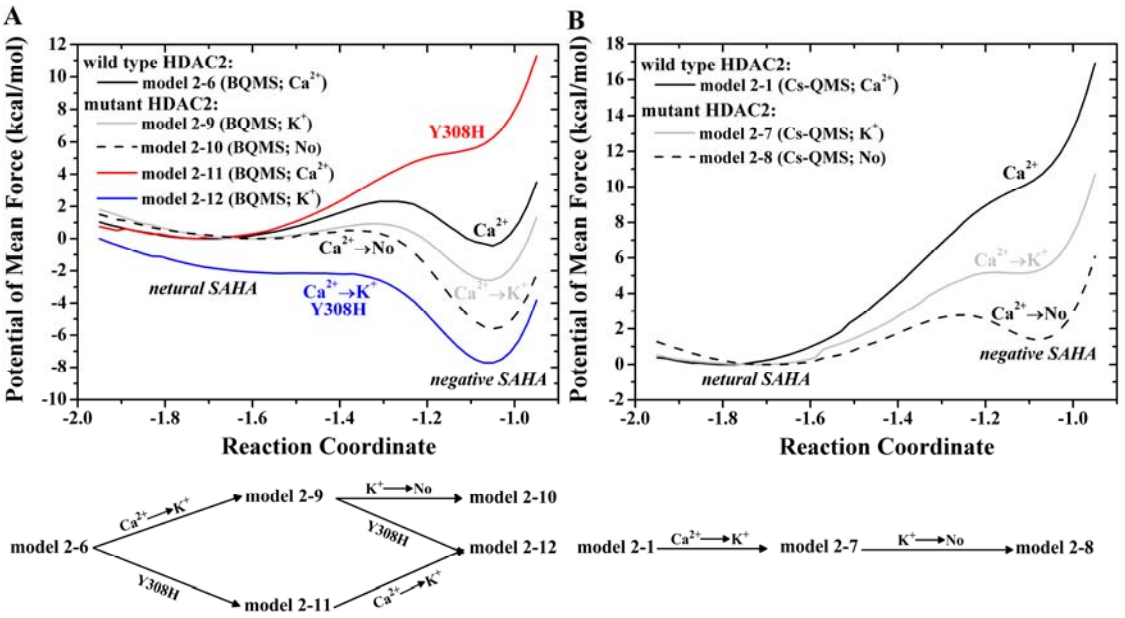

Figure S5. The comparison of free energy profiles for wild/mutant type HDAC2 based on the BQMS (A) and Cs-QMS (B) which refer to Figure 2 (c), Table S2-S3 and Figure S2. The distance between the hydroxyl hydrogen of SAHA and the N^{ε} atom of H145 is chosen as the reaction coordinate.

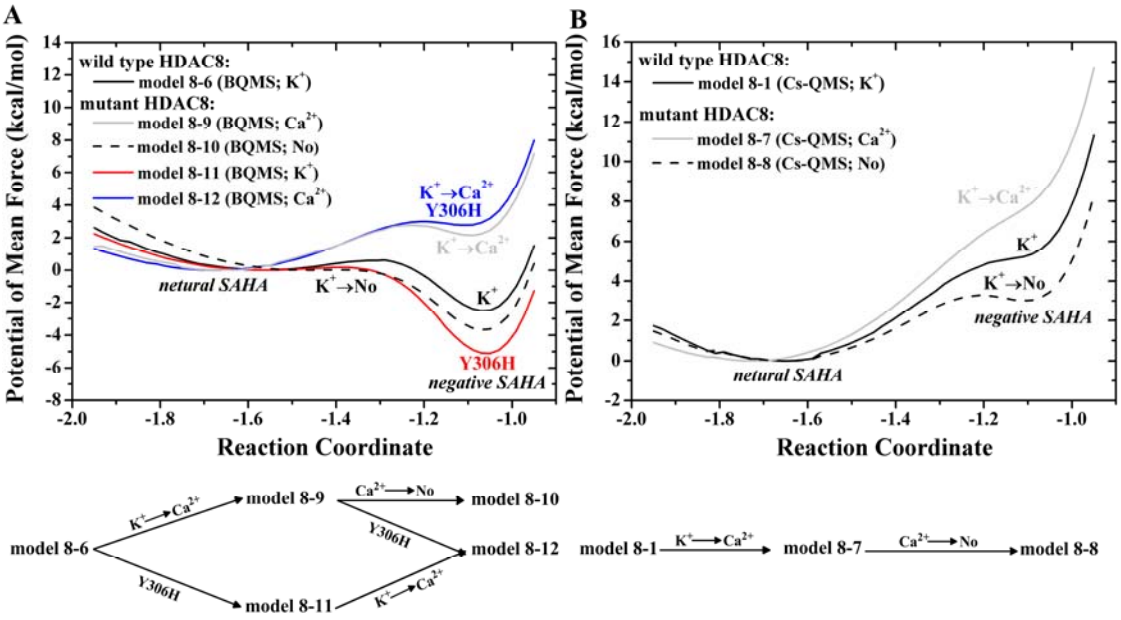

Figure S6. The comparison of free energy profiles for wild/mutant type HDAC8 based on the BQMS (A) and Cs-QMS (B) which refer to Figure 2 (d), Table S4-S5 and Figure S2. The distance between the hydroxyl hydrogen of SAHA and the N^{ε} atom of H142 is chosen as the reaction coordinate.

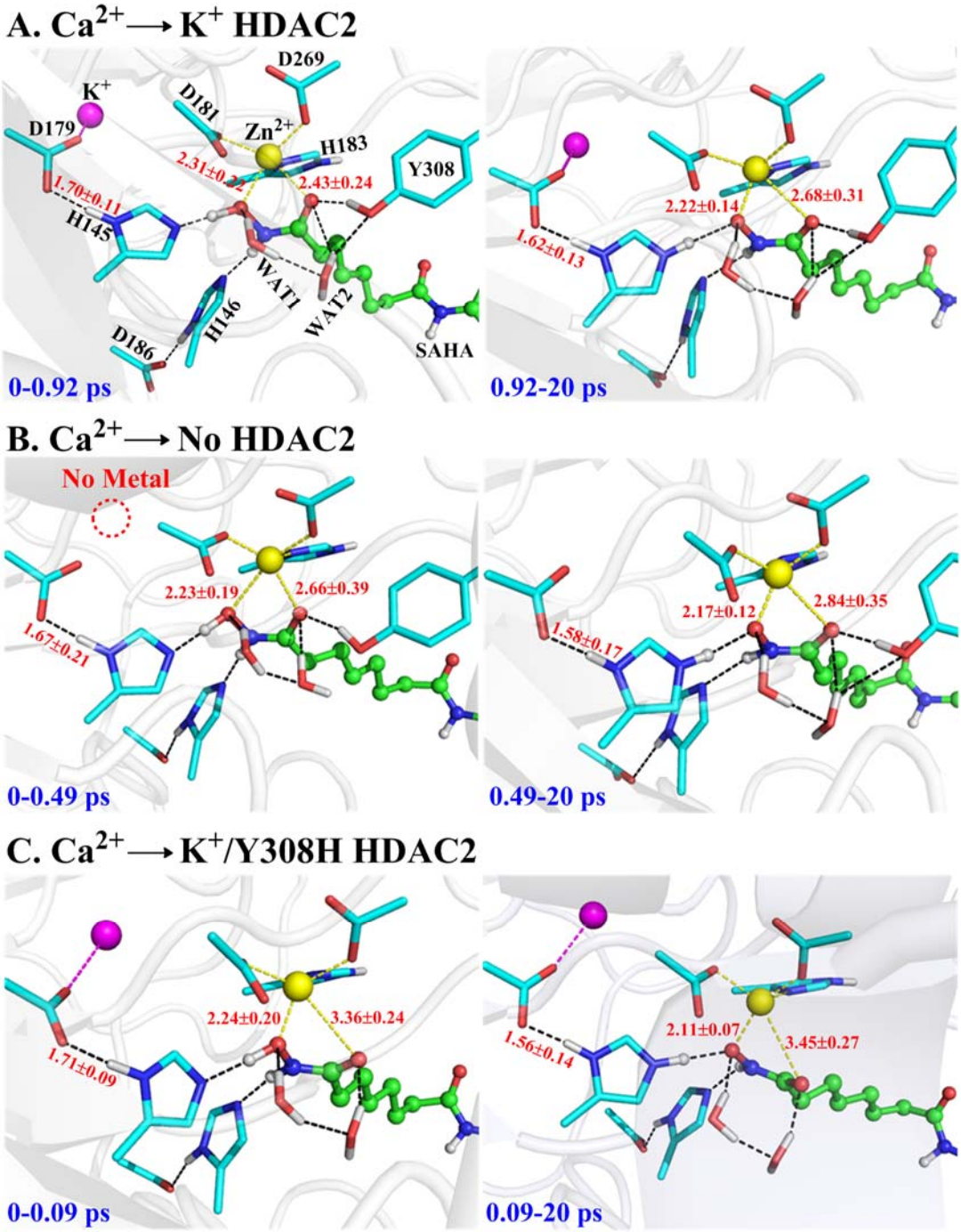

Figure S7. The variation of the active site structures along the 20 ps unrestricted QM/MM MD simulations for the mutant HDAC2-SAHA models in which the metal ion in "the second metal site" are mutated to be K^+ ion or deleted. The variations of the models with Ca^{2+} ion (wild type) were shown in Figure 3. The survival time (ps) of the neutral and negative SAHA colored in blue refer to Table S7.

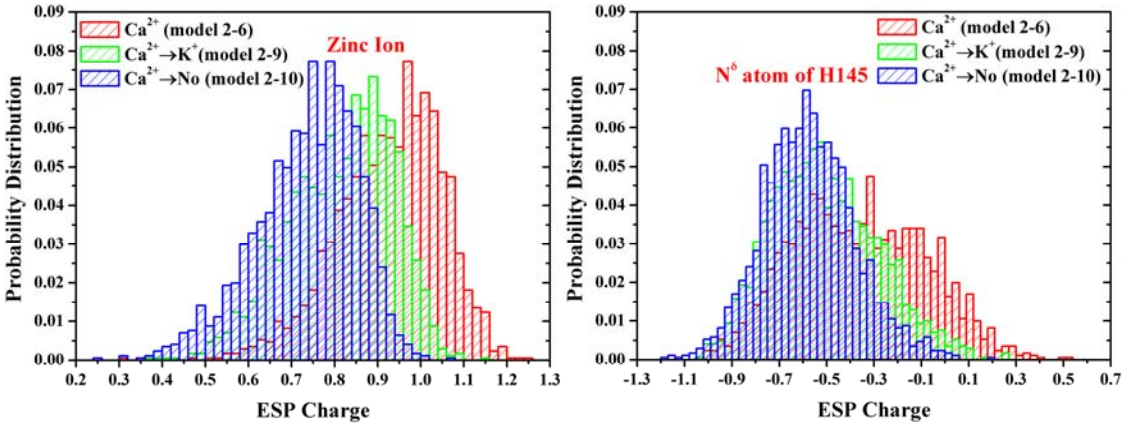

Figure S8. The comparison of the ESP charge (Zinc ion and H145:N^{δ}) in the reactant state (Neutral SAHA) along the proton transfer reaction among the HDAC2 models (model 2-6, model 2-9 and model 2-10, see Table S2 and S3) in which the metal ions in "the second metal site" are different.

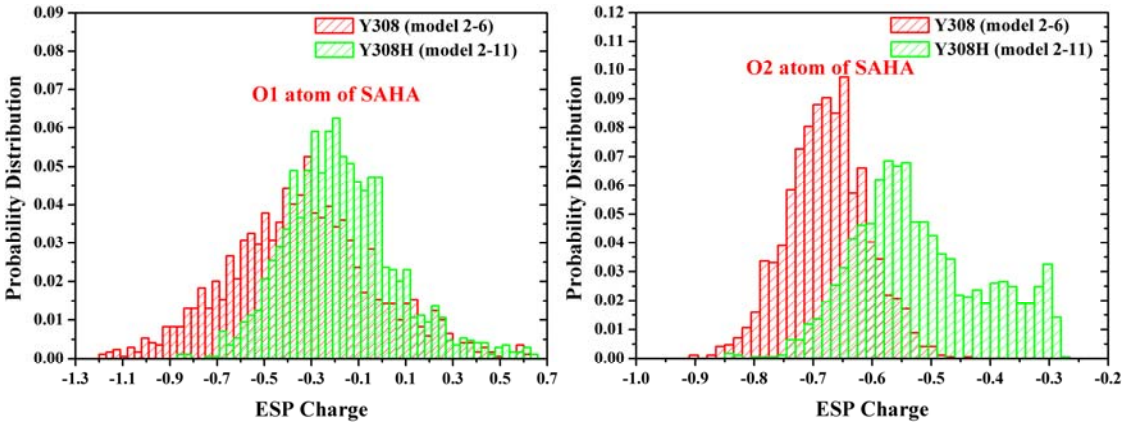

Figure S9. The comparison of the ESP charge (SAHA: O1 and SAHA: O2, O1 and O2 are the hydroxyl oxygen and the ketonic oxygen of SAHA, respectively, see Figure 1) in the reactant state (Neutral SAHA) of the proton transfer reaction between the wild type HDAC2 models (model 2-6, see Table S2) and the Y308H HDAC2 mutant model (model 2-11, see Table S3).

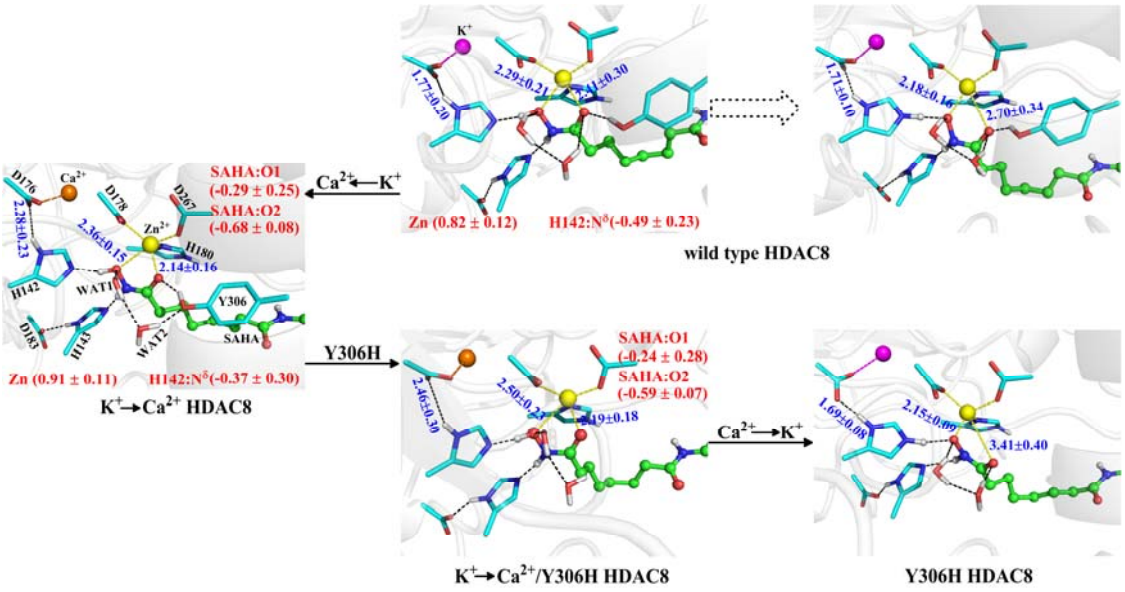

Figure S10. The remote "second metal site" dependent (namely "Metal-dependent") regulatory effect on the deprotonation of SAHA as well as functional role of Y306 in HDAC8. More detailed structure evolution and ESP charge analysis are provided in Figure S11-S13. The similar conclusion could be found for HDAC2, as shown in Figure 3.

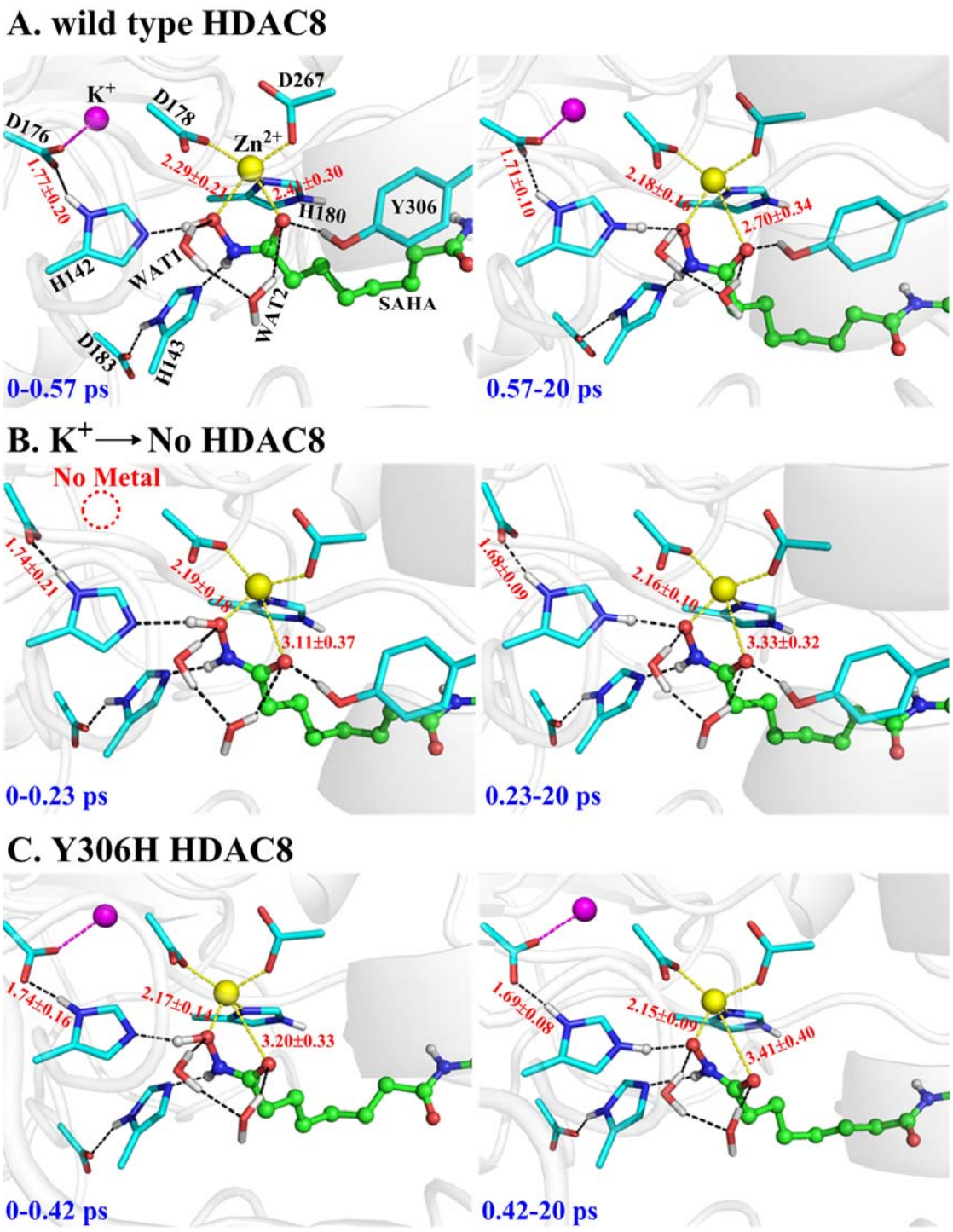

Figure S11. The variation of the active site structures along the 20 ps unrestricted QM/MM MD simulations for the HDAC8-SAHA models in which the metal ion in "the second metal site" are K^+ ion or nonexistent. The variations of the models with Ca^{2+} ion were shown in Figure S10. The survival time (ps) of the neutral and negative SAHA colored in blue refer to Table S7.

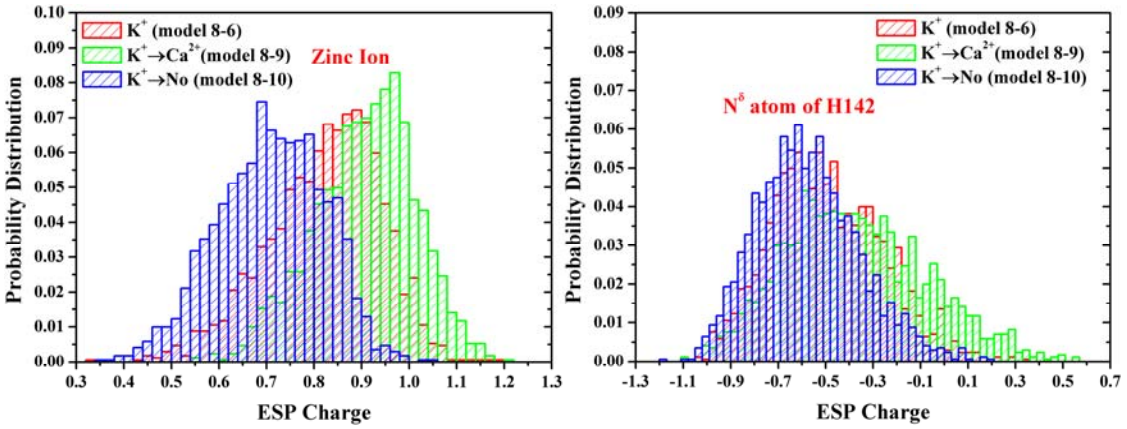

Figure S12. The comparison of the ESP charge (Zinc ion and H142: N^{δ}) in the reactant state (Neutral SAHA) along the proton transfer reaction among the HDAC8 models (model 8-6, model 8-9 and model 8-10, see Table S4 and S5) in which the metal ions in "the second metal site" are different.

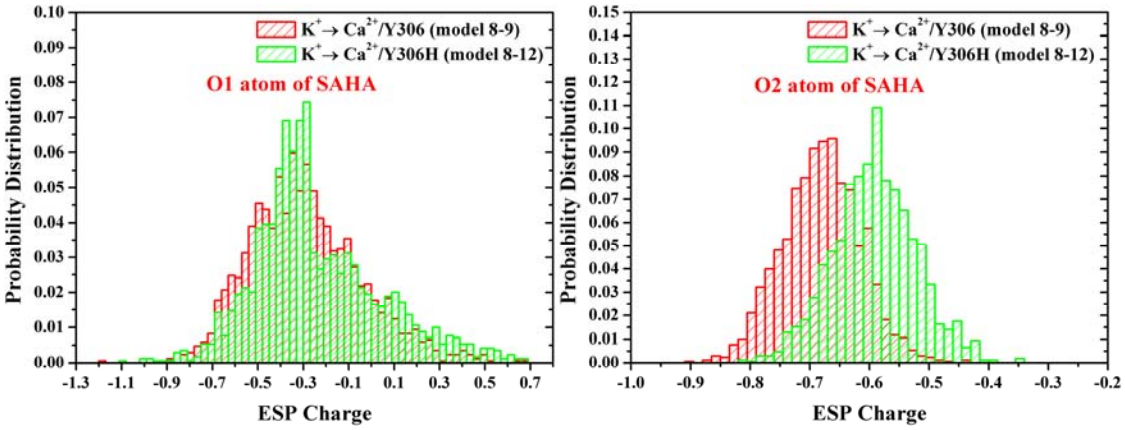

Figure S13. The comparison of the ESP charge (SAHA: O1 and SAHA: O2, O1 and O2 are the hydroxyl oxygen and the ketonic oxygen of SAHA, respectively, see Figure 1) in the reactant state (Neutral SAHA) of the proton transfer reaction between the $K^+ \rightarrow Ca^{2+}$ single HDAC8 mutant model (model 8-9, see Table S5) and the $K^+ \rightarrow Ca^{2+}$/Y306H double HDAC8 mutant model (model 8-12, see Table S5).

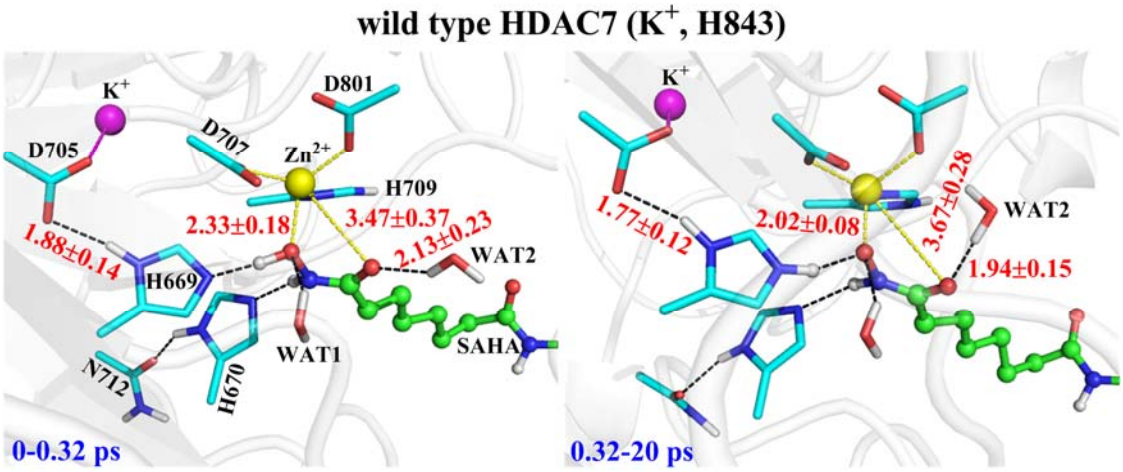

Figure S14. The variation of the active site structures along the 20 ps unrestricted QM/MM MD simulations for the wild type HDAC7-SAHA models (model 7-2, refer to Table S6) in which the Tyr residue is replaced by H843 and the metal ion in "the second metal site" is K^+ ion. The survival time (ps) of the neutral and negative SAHA colored in blue refer to Table S7.

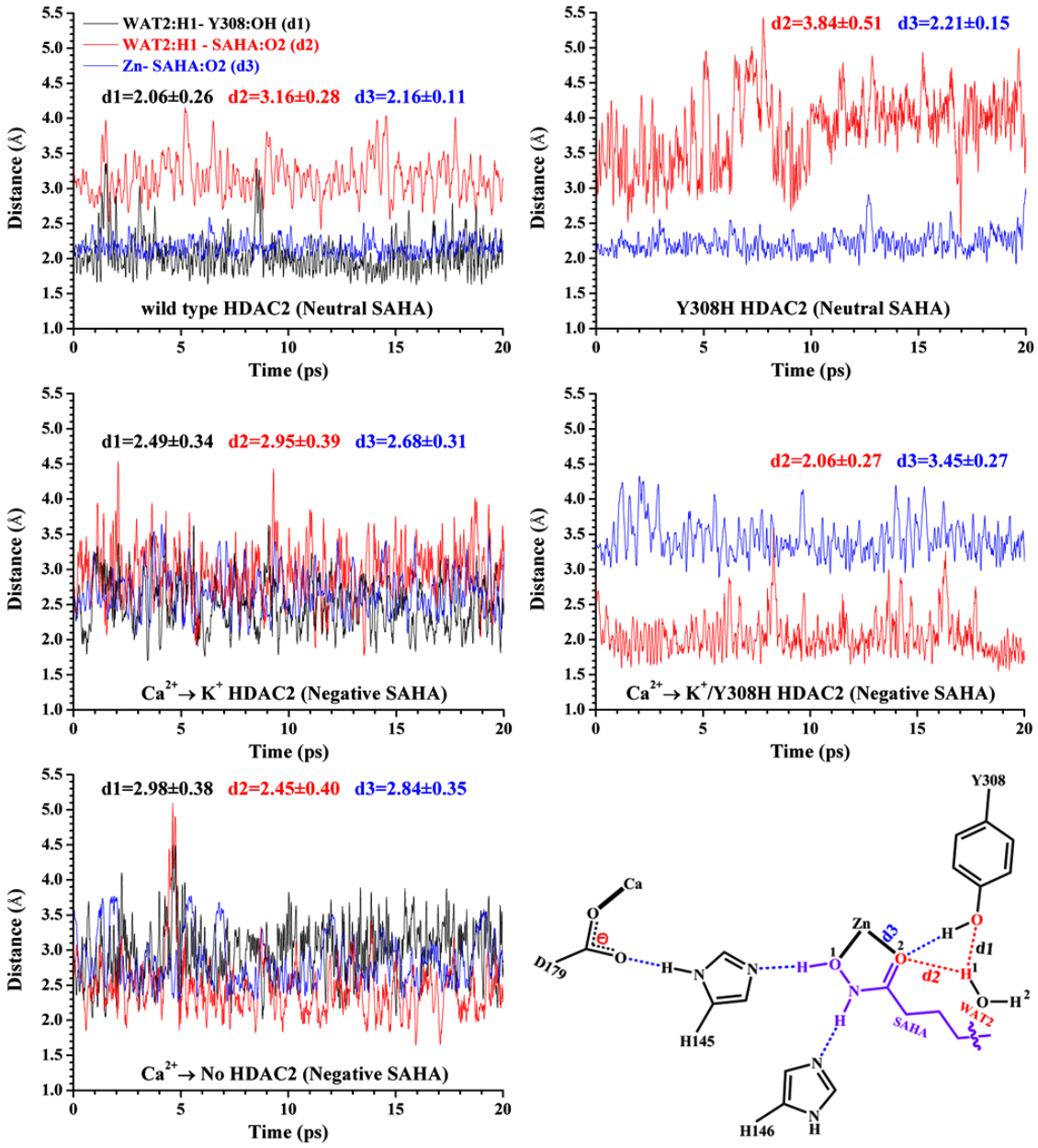

Figure S15. The distance evolution of the important hydrogen bonds WAT2:H1-Y308: OH (d1), WAT2:H1-SAHA: O2 (d2) and Zn-SAHA: O2 (d3) during the 20 ps unrestricted QM/MM MD simulation in wild and mutant HDAC2. All data are also summarized in Table S8.

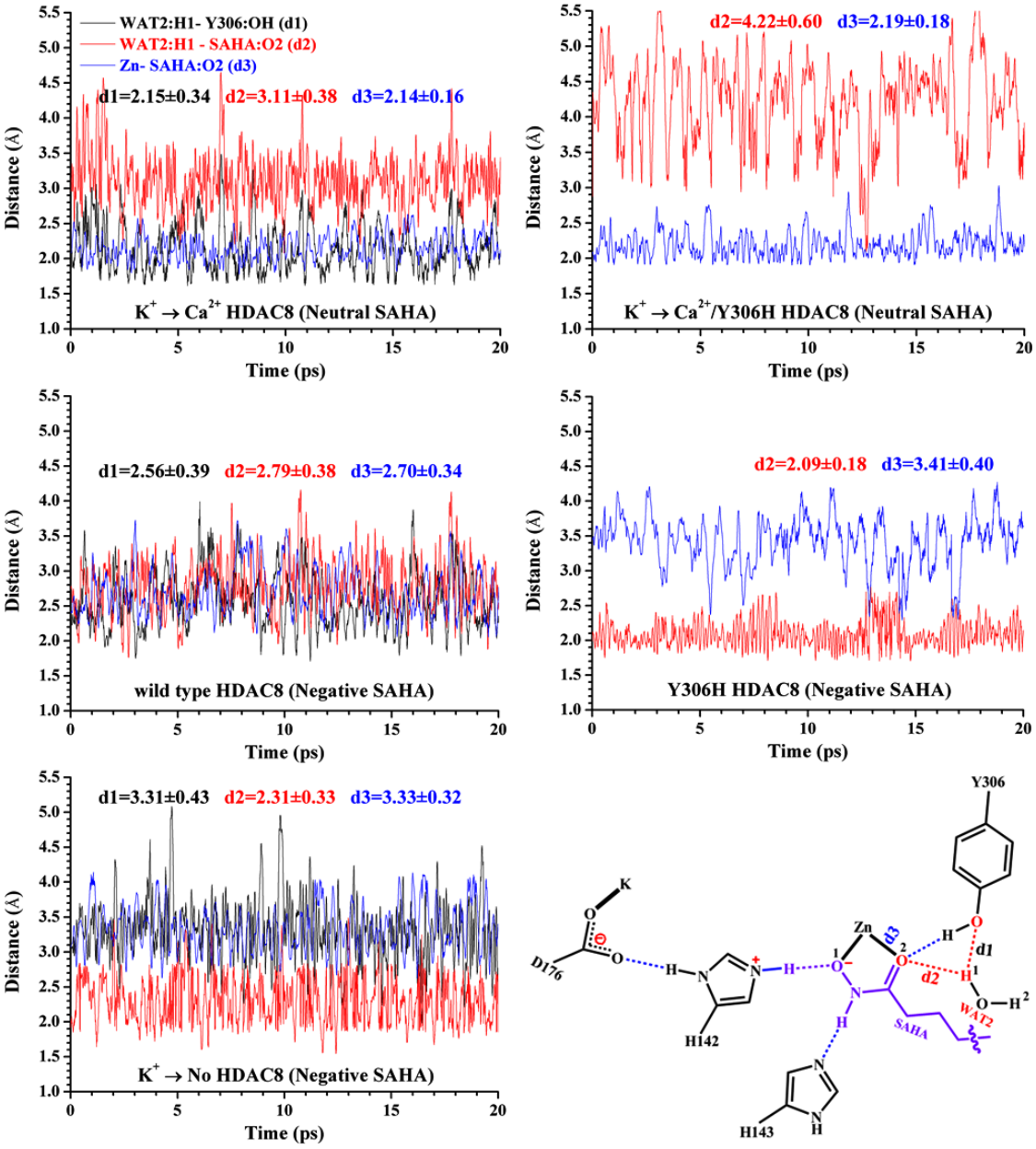

Figure S16. The distance evolution of the important hydrogen bonds WAT2:H1-Y306: OH (d1), WAT2:H1-SAHA: O2 (d2) and Zn-SAHA: O2 (d3) during the 20 ps unrestricted QM/MM MD simulation in wild and mutant HDAC8. All data are also summarized in Table S8.

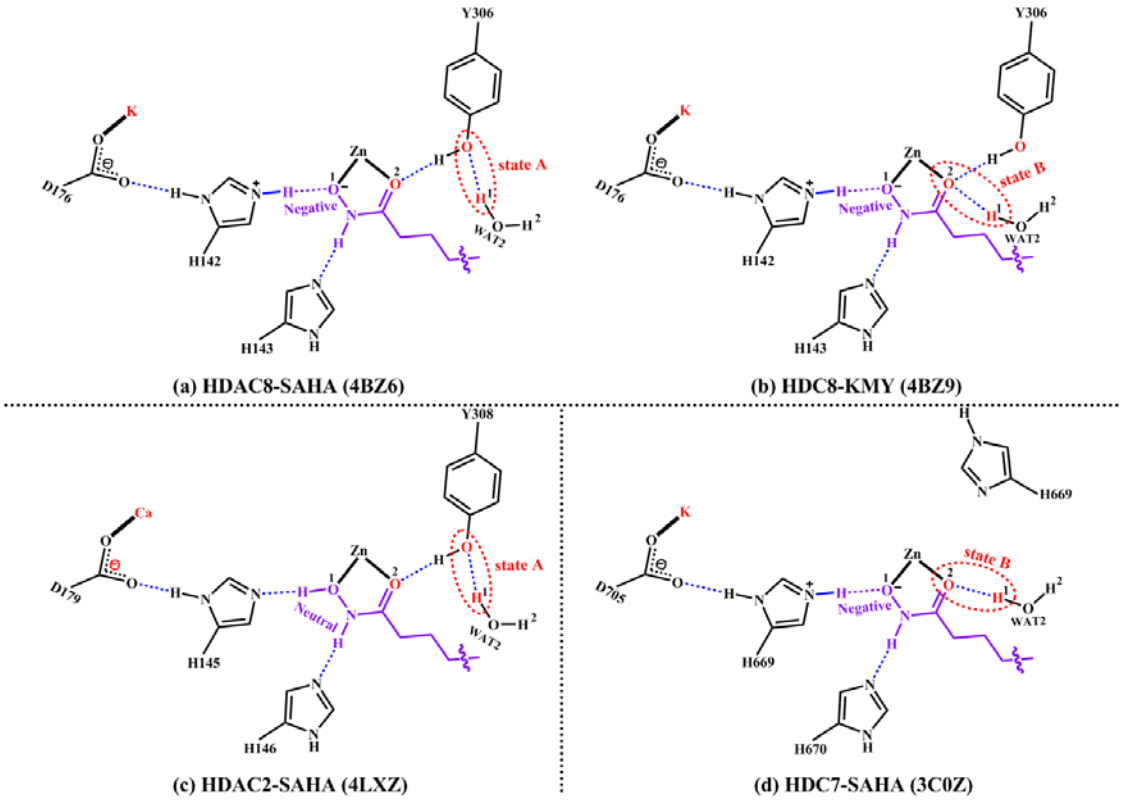

Figure S17. The hydrogen bond network around the WAT2 in the HDAC8/2/7-hydroxamate crystal structures. For HDAC8, WAT2 could form hydrogen bond with either Y306: OH or SAHA: O2. Therefore, two states (state A and state B) were found in the HDAC8 crystal structures (a & b). While for HDAC2 and HDAC7, only state A and state B were found in the crystal structure, respectively (c and d). 4BZ7 (HDAC8-B3N) which is similar to 4BZ6 also tends to be state A and 3C10 (HDAC7-TSA) which is similar to 3C0Z also tends to be state B. Thus they are not shown here. B3N, KMY and TSA are SAHA-like inhibitors. 4BZ6, 4BZ7 and 4BZ9 crystals are *schistosoma mansoni* HDAC8 whose active sites are identical with human HDAC8.

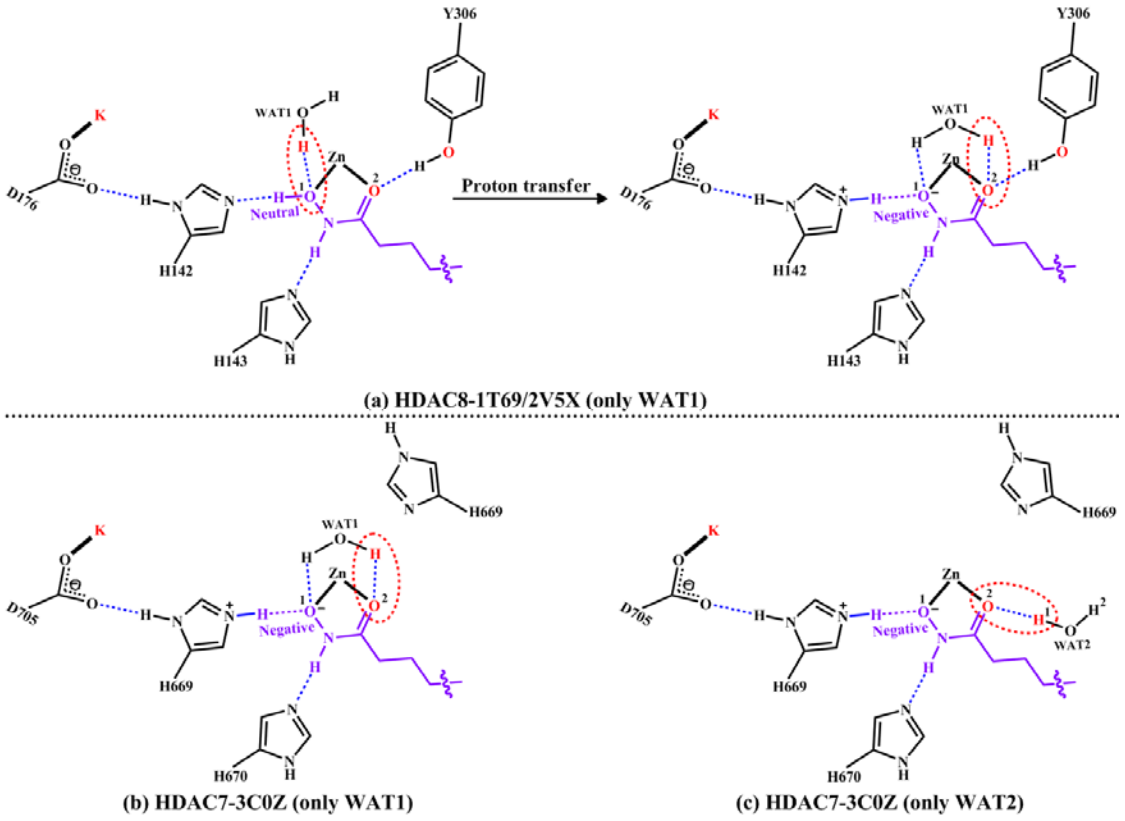

Figure S18. The hydrogen bond network around WAT1 in the HDAC8/7-SAHA crystal structures (only WAT1 or WAT2). For HDAC8/7 (only WAT1), WAT1 could form hydrogen bond with both SAHA: O1 or SAHA: O2 when the proton was transferred to H142/H669 (a and b). While for HDAC7 (only WAT2), the WAT2 just form hydrogen bond with SAHA: O2. It indicated that the WAT1 would also play the functional role (form hydrogen bond with SAHA: O2) to promote the proton transfer reaction even if WAT2 was removed. The HDAC8-1T69/2V5X (only WAT1), HDAC7-3C0Z (only WAT1) and HDAC7-3C0Z (only WAT2) refer to Table S10.

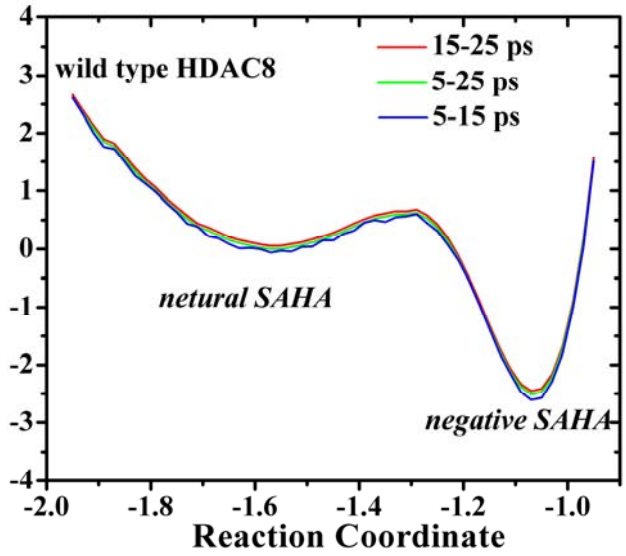

Figure S19. The convergence of the computational free energy profile. It indicates that our one-dimensional free energy profile is reliable.

Table S1. The coordination distances of Zn-SAHA: O1 and Zn-SAHA: O2 as well as the resident water of the second zinc coordination shell in the all available crystals for HDAC8/7/2-hydroxamate complexes. The ligands—B3N, TSA, KMY, CRI, J38, V5X and NHB are similar to SAHA structurally. 4BZ6-4BZ9 crystals are *schistosoma mansoni* HDAC8 whose active sites are identical with human.

PDB ID	Ligand	Resolution	WAT	d(Zn-SAHA:O1)	d(Zn-SAHA:O2)
HDAC8					
4BZ7	B3N	1.65	WAT1/2	2.04 2.04 2.04 2.06	2.35 2.44 2.35 2.33
3EW8	B3N	1.80	/	2.53	2.29
3MZ4	B3N	1.85	/	1.94 2.27	2.35 2.25
3MZ7	B3N	1.90	/	1.82	2.43
1T64	TSA	1.90	/	2.03 2.00	2.32 2.22
3MZ6	B3N	2.00	/	1.91	2.61
4BZ6	SAHA	2.00	WAT1/2	2.19 2.17 2.12 2.10	2.34 2.47 2.34 2.35
4BZ9	KMY	2.00	WAT1/2	2.38 2.10 2.24 2.01	3.01 2.52 2.87 2.77
1VKG	CRI	2.20	WAT1	1.97	1.91
4BZ8	J38	2.21	WAT1	2.37 2.43 2.31 2.47	2.91 2.67 2.72 2.68
2V5X	V5X	2.25	WAT1	2.16 2.08	2.29 2.25
1T67	B3N	2.31	/	1.99	2.03
1W22	NHB	2.50	WAT1	2.16 2.14	2.17 2.50
3F0R	TSA	2.54	/	2.49 2.19 2.39	2.27 2.18 2.23
3F06	B3N	2.55	/	2.12 1.94	1.95 2.10
3EZP	B3N	2.65	/	2.03 2.35	2.02 2.23
3EZT	B3N	2.85	/	2.29	2.30

				2.31	2.24
1T69	SAHA	2.91	/	1.95	1.97
3MZ3	B3N	3.20	/	2.18 2.33	2.44 2.51
HDAC7					
3C10	TSA	2.00	WAT2	1.99 2.14	2.66 2.58
3C0Z	SAHA	2.10	WAT2	2.07 2.33	2.85 2.72
HDAC2					
4LXZ	SAHA	1.85	WAT1/2	2.38 2.33 2.42	2.05 1.96 1.98

Table S2. The illustration of the detailed QM subsystems and the free energy of the transition state (TS) and product state (Negative SAHA) of the proton transfer reaction in the HDAC2-SAHA wild type models.

Models	Metal Ion	Water	QM Region	Free Energy (kcal/mol)	
				TS	Negative SAHA
Model 2-1 (HDAC2)	Ca^{2+}	No	Zn^{2+}; SAHA; D181; H183; D269; H145; H146.	> 10	> 10
Model 2-2 (HDAC2)	Ca^{2+}	No	Zn^{2+}; SAHA; D181; H183; D269; H145; H146; D179; D186.	5.3±0.1	5.3±0.1
Model 2-3 (HDAC2)	Ca^{2+}	Yes	Zn^{2+}; SAHA; D181; H183; D269; H145; H146.	7.7±0.1	7.6±0.1
Model 2-4 (HDAC2)	Ca^{2+}	Yes	Zn^{2+}; SAHA; D181; H183; D269; H145; H146; D179; D186.	4.2±0.1	2.1±0.1
Model 2-5 (HDAC2)	Ca^{2+}	Yes	Zn^{2+}; SAHA; D181; H183; D269; H145; H146; D179; D186; WAT1; WAT2.	2.5±0.1	-0.2±0.2
Model 2-6 (HDAC2)	Ca^{2+}	Yes	Zn^{2+}; SAHA; D181; H183; D269; Y308; H145; H146; D179; D186; WAT1; WAT2.	2.3±0.1	-0.4±0.2

Table S3. The illustration of the detailed QM subsystems and the free energy of the transition state (TS) and product state (Negative SAHA) of the proton transfer reaction in the Ca^{2+}→K^{+}/Ca^{2+}→No/Y308H HDAC2-SAHA mutant models.

Models	Metal Ion	Water	QM Region	Free Energy (kcal/mol)	
				TS	Negative SAHA
Model 2-7 (HDAC2)	K^{+}	No	Zn^{2+}; SAHA; D181; H183; D269; H145; H146.	5.2±0.1	5.1±0.1
Model 2-8 (HDAC2)	No	No	Zn^{2+}; SAHA; D181; H183; D269; H145; H146.	2.8±0.1	1.4±0.2
Model 2-9 (HDAC2)	K^{+}	Yes	Zn^{2+}; SAHA; D181; H183; D269; Y308; H145; H146; D179; D186; WAT1; WAT2.	0.9±0.1	-2.6±0.1
Model 2-10 (HDAC2)	No	Yes	Zn^{2+}; SAHA; D181; H183; D269; Y308; H145; H146; D179; D186; WAT1; WAT2.	0.5±0.1	-5.6±0.1
Model 2-11 (HDAC2)	Ca^{2+}	Yes	Zn^{2+}; SAHA; D181; H183; D269; H308; H145; H146; D179; D186; WAT1; WAT2.	5.5±0.1	5.5±0.1
Model 2-12 (HDAC2)	K^{+}	Yes	Zn^{2+}; SAHA; D181; H183; D269; H308; H145; H146; D179; D186 WAT1; WAT2.	0	-7.7±0.2

Table S4. The illustration of the detailed QM subsystems and the free energy of the transition state (TS) and product state (Negative SAHA) of the proton transfer reaction in the HDAC8-SAHA wild type models.

Models	Metal Ion	Water	QM Region	Free Energy (kcal/mol)	
				TS	Negative SAHA
Model 8-1 (HDAC8)	K^+	No	Zn^{2+}; SAHA; D178; H180; D267; H142; H143.	5.1±0.1	5.1±0.1
Model 8-2 (HDAC8)	K^+	No	Zn^{2+}; SAHA; D178; H180; D267; H142; H143; D176; D183.	3.3±0.1	3.3±0.1
Model 8-3 (HDAC8)	K^+	Yes	Zn^{2+}; SAHA; D178; H180; D267; H142; H143.	2.7±0.1	1.4±0.2
Model 8-4 (HDAC8)	K^+	Yes	Zn^{2+}; SAHA; D178; H180; D267; H142; H143; D176; D183.	2.2±0.1	1.1±0.2
Model 8-5 (HDAC8)	K^+	Yes	Zn^{2+}; SAHA; D178; H180; D267; H142; H143; D176; D183; WAT1; WAT2.	0.8±0.1	-2.3±0.2
Model 8-6 (HDAC8)	K^+	Yes	Zn^{2+}; SAHA; D178; H180; D267; Y306; H142; H143; D176; D183; WAT1; WAT2.	0.6±0.1	-2.5±0.1

Table S5. The illustration of the detailed QM subsystems and the free energy of the transition state (TS) and product state (Negative SAHA) of the proton transfer reaction in the $K^+ \rightarrow Ca^{2+}$/$K^+ \rightarrow$No/Y306H HDAC8-SAHA mutant models.

Models	Metal Ion	Water	QM Region	Free Energy (kcal/mol)	
				TS	Negative SAHA
Model 8-7 (HDAC8)	Ca^{2+}	No	Zn^{2+}; SAHA; D178; H180; D267; H142; H143.	> 10	> 10
Model 8-8 (HDAC8)	No	No	Zn^{2+}; SAHA; D178; H180; D267; H142; H143.	3.3±0.1	3.0±0.1
Model 8-9 (HDAC8)	Ca^{2+}	Yes	Zn^{2+}; SAHA; D178; H180; D267; Y306; H142; H143; D176; D183; WAT1; WAT2.	2.8±0.1	2.2±0.1
Model 8-10 (HDAC8)	No	Yes	Zn^{2+}; SAHA; D178; H180; D267; Y306; H142; H143; D176; D183; WAT1; WAT2.	0	-3.7±0.1
Model 8-11 (HDAC8)	K^+	Yes	Zn^{2+}; SAHA; D178; H180; D267; H306; H142; H143; D176; D183; WAT1; WAT2.	0.2±0.1	-5.1±0.2
Model 8-12 (HDAC8)	Ca^{2+}	Yes	Zn^{2+}; SAHA; D178; H180; D267; H306; H142; H143; D176; D183; WAT1; WAT2.	3.0±0.1	2.8±0.1

Table S6. The illustration of the detailed QM subsystems and the free energy of the transition state (TS) and product state (Negative SAHA) of the proton transfer reaction in the HDAC7-SAHA models (model 7-1, 7-2 and 7-3). The Biggest QM Subsystem (BQMS) was chosen for the three models. The differences among the three models are the water of the second zinc coordination shell (complete WAT1/2 for model 7-2, while only WAT1 or WAT2 for model 7-1 or model 7-3, respectively).

Models	Metal Ion	Water	QM Region	Free Energy (kcal/mol)	
				TS	Negative SAHA
Model 7-1 (HDAC7)	K^+	Only WAT2	Zn^{2+}; SAHA; D707; H709; D801; H843; H669; H670; D705; N712; WAT2.	0.7±0.1	-3.1±0.1
Model 7-2 (HDAC7)	K^+	Yes	Zn^{2+}; SAHA; D707; H709; D801; H843; H669; H670; D705; N712; WAT1; WAT2.	0.3±0.1	-4.4±0.1
Model 7-3 (HDAC7)	K^+	Only WAT1	Zn^{2+}; SAHA; D707; H709; D801; H843; H669; H670; D705; N712; WAT2.	1.1±0.2	-1.7±0.1

Table S7. The survival time (ps) of the neutral and negative SAHA during the 20 ps unrestricted QM/MM MD simulation. All the models refer to Table S2-S6, and the BQMS are chosen as their QM subsystems.

Models	Metal Ion	TYR(Y)/HIS(H)	Survival Time (ps)	
			Neutral SAHA	Negative SAHA
Model 2-6 (HDAC2)	Ca^{2+}	Y308	0—20	/
Model 2-9 (HDAC2)	K^{+}	Y308	0—0.92	0.92—20
Model 2-10 (HDAC2)	No	Y308	0—0.49	0.49—20
Model 2-11 (HDAC2)	Ca^{2+}	H308	0—20	/
Model 2-12 (HDAC2)	K^{+}	H308	0—0.09	0.09—20
Model 8-6 (HDAC8)	K^{+}	Y306	0—0.57	0.57—20
Model 8-9 (HDAC8)	Ca^{2+}	Y306	0—20	/
Model 8-10 (HDAC8)	No	Y306	0—0.23	0.23—20
Model 8-11 (HDAC8)	K^{+}	H306	0—0.42	0.42—20
Model 8-12 (HDAC8)	Ca^{2+}	H306	0—20	/
Model 7-2 (HDAC7)	K^{+}	H843	0—0.32	0.32—20

Table S8. The distance evolution of the Zn-SAHA:O2 (d3), WAT2:H1-SAHA:O2 (d2) and WAT2:H1-Y308(306):OH (d1) during the 20 ps unrestricted QM/MM MD simulation in HDAC2, HDAC8 and HDAC7. The detailed evolution curves were shown in Figure S15 and Figure S16. All the models refer to Table S2-S6, and the BQMS are chosen as their QM subsystems. d1-d3 refer to Figure S15-S16.

Models	Zn-SAHA:O2 (d3)	WAT2:H1-SAHA:O2 (d2)	WAT2:H1-Y308(306):OH (d1)
Model 2-6 (wild type)	2.16 ± 0.11	3.16 ± 0.28	2.06 ± 0.26
Model 2-9 (Ca^{2+}→K^{+})	2.68 ± 0.31	2.95 ± 0.39	2.49 ± 0.34
Model 2-10 (Ca^{2+}→No)	2.84 ± 0.35	2.45 ± 0.40	2.98 ± 0.38
Model 2-11 (Y308H)	2.21 ± 0.15	3.84 ± 0.51	/
Model 2-12 (Ca^{2+}→K^{+}/ Y308H)	3.45 ± 0.27	2.06 ± 0.27	/
Model 8-6 (wild type)	2.70 ± 0.34	2.79 ± 0.38	2.56 ± 0.39
Model 8-9 (K^{+}→Ca^{2+})	2.14 ± 0.16	3.11 ± 0.38	2.15 ± 0.34
Model 8-10 (K^{+}→No)	3.33 ± 0.32	2.31 ± 0.33	3.31 ± 0.43
Model 8-11 (Y306H)	3.41 ± 0.40	2.09 ± 0.18	/
Model 8-12 (K^{+}→Ca^{2+}/ Y306H)	2.19 ± 0.18	4.22 ± 0.60	/
Model 7-2 (wild type)	3.67 ± 0.28	1.94 ± 0.15	/

Table S9. The comparison of the coordination distances (Zn-SAHA:O1 and Zn-SAHA:O2) between the crystals and calculative structures. The ligands for HDAC8/7/2 are SAHA (4BZ6, 3C0Z and 4LXZ), B3N (4BZ7), KMY (4BZ9) and TSA (3C10). The structures of SAHA, B3N, KMY and TSA are very similar and they all belong to hydroxamic acid. 4BZ6, 4BZ7 and 4BZ9 crystals are *schistosoma mansoni* HDAC8 whose active sites are identical with human HDAC8. State A and State B refer to Figure S17.

Structure		Resolution	d(Zn-SAHA:O1)	d(Zn-SAHA:O2)
HDAC8				
Crystal	**4BZ6 (State A)**	2.00	2.19 2.17 2.12 2.10	2.34 2.47 2.34 2.35
	4BZ7 (State A)	1.65	2.04 2.04 2.04 2.06	2.35 2.44 2.35 2.33
	4BZ9 (State B)	2.00	2.38 2.10 2.24 2.01	3.01 2.52 2.87 2.77
Calc	**Neutral SAHA**	/	2.29 ± 0.21	2.41 ± 0.30
	Negative SAHA	/	2.18 ± 0.16	2.70 ± 0.34
HDAC7				
Crystal	**3C10 (state B)**	2.00	1.99 2.14	2.66 2.58
	3C0Z (state B)	2.10	2.07 2.33	2.85 2.72
Calc	**Neutral SAHA**	/	2.33 ± 0.18	3.47 ± 0.37
	Negative SAHA	/	2.02 ± 0.08	3.67 ± 0.28
HDAC2				
Crystal	**4LXZ (state A)**	1.85	2.38 2.33 2.42	2.05 1.96 1.98
Calc	**Neutral SAHA**	/	2.32 ± 0.17	2.16 ± 0.11
	Negative SAHA	/	2.08 ± 0.09	2.33 ± 0.18

Table S10. The survival time (ps) of the neutral and negative SAHA during the 20 ps unrestricted QM/MM MD simulation. The BQMS are chosen as their QM subsystems . The differences among these models are the water molecules (WAT1/2) in the second zinc coordination shell. The HDAC8-1T69 (WAT1/2), HDAC7-3C0Z (WAT1/2), HDAC7-3C0Z (only WAT1) and HDAC7-3C0Z (only WAT2) refer to model 8-6, 7-2, 7-3 and 7-1, respectively.

Models	Metal Ion	TYR(Y)/HIS(H)	Survival Time (ps)	
			Neutral SAHA	Negative SAHA
HDAC8-1T69 (WAT1/2)	K^+	Y306	0—0.57	0.57—20
HDAC8-1T69 (only WAT1)	K^+	Y306	0—2.12	2.12—20
HDAC8-1T69 (no WAT1/2)	K^+	Y306	0—20	/
HDAC8-2V5X (WAT1/2)	K^+	Y306	0—0.64	0.64—20
HDAC8-2V5X (only WAT1)	K^+	Y306	0—2.36	2.36—20
HDAC8-2V5X (no WAT1/2)	K^+	Y306	0—20	/
HDAC7-3C0Z (WAT1/2)	K^+	H843	0—0.32	0.32—20
HDAC7-3C0Z (only WAT1)	K^+	H843	0—1.24	1.24—20
HDAC7-3C0Z (only WAT2)	K^+	H843	0—0.47	0.47—20